Effect of Si and Ge doping on electronic structure of InP nanowire

SENA GULER OZKAPI[1,*], BARIS OZKAPI[1], ALI IHSAN MESE[2], ILHAN ERDOGAN[2]
[1]*Trakya University, Edirne Vocational School of Technical Sciences, 22030, Edirne, Türkiye*
[2]*Trakya University, Department of Physics, 22030, Edirne, Türkiye*

We present a study on the effect of Si and Ge doping on the electronic and atomic structure of Indium Phosphide nanowires using first principles calculations. Hydrogen passivated InP nanowires in zinc blende structure with 1.5 nanometers diameter [111] growth direction are considered. The results show that the substitutional Si and Ge dopings narrow the band gap of InP nanowires, and these nanowires are direct band gap semiconductors. The Si doping shifts the VBM and CBM to the lower energy levels, and this energy decrease is less in the Ge doped nanowire. PDOS analyses show that VBM and CBM occur mainly from the p orbitals of the In and P atoms. Electronic states at the Fermi level for doped nanowires are compatible with the donor levels that appear in the band structure.

(Received June 6, 2023; accepted November 24, 2023)

Keywords: InP nanowire, Zinc blende, DFT calculation, Si doping, Ge doping

1. Introduction

Semiconductor nanowires (NWs) have favorable characteristics and great potential for nanoelectronics, thermoelectrics, and photonics [1-3]. The electronic, optical, and mechanical properties of nanowires called one-dimensional nanostructures differ from their bulk types. In order to understand the advantages of the reduced dimensionality and size, nanowires can be varied in different geometry, shape, and diameter [4-7]. Besides, it is known that adding foreign atoms to nanowires changes many properties in these structures [8-12].

III-V materials play an important role in advanced technology on electronic devices such as light emitting diodes, optoelectronic devices, and photovoltaic materials. Compared with other III-V compounds, Indium Phosphide (InP) is one of the most attractive materials in the III-V group, which is used in high frequency and high power electronic devices due to superior electron velocities [13, 14]. Many theoretical and experimental studies have been carried out to understand the structural and electronic properties of InP nanowires. Experimental methods such as chemical beam epitaxy, metal-organic vapor epitaxy, and laser ablation have been used to synthesize for InP nanowires [15-18]. In another experimental study, it has been presented that the band gap increases as the diameter of the nanowire decreases [19]. Vapor liquid solid and selective area epitaxy has been used to produce wurtzite InP nanowire with good optical properties [20, 21]. The optical properties of InP nanowires with wurtzite and zinc blende phases have been studied [22, 23]. The adjusting of the nanowire by changing the nanowire diameter and concentration of dopant has been presented [24, 25]. The Young's modulus of InP nanowire has been found via a developed scanning probe microscopy approach [26]. The structural, optic, and elastic properties of InP nanowires and the effect of nanowire diameter have been demonstrated [27, 28]. Theoretically, first principles calculations of InP nanowires have been performed. The electronic properties of zinc-blende, wurtzite, and rotationally twinned InP nanowires have been studied. It has been found that all the nanowires show a semiconducting character, and the band gap decreases with increasing the nanowire size [29]. The electronic and mechanical properties of zinc blende InP nanowires have been calculated. The lattice constants of the nanowires have been determined to decrease with decreasing diameter due to the shorter surface lattice constant of the nanowires when compared to their bulk values. It has been declared that Young's modulus decreases, whereas the Poisson ratio increases as the wire radius decreases for the InP nanowire [6].

For the most part, the surface of the semiconductor nanostructure is passivated due to the effect of the dangling bonds. Unless the nanostructure is passivated, the dangling bonds of the surface atoms constitute electronic levels near the Fermi energy, and these levels spoil the electronic and optic properties of the nanostructure. Akiyama et al. have shown that the surface dangling bonds on the wurtzite InP nanowire facets play a crucial role in stabilizing [30]. Moreira et al. have passivated the surface of InP nanowires in several ways using OH radicals and found that the exchange of atoms is energetically favorable, and dangling bonds are more stable [31]. In addition to these studies, the effect of doping and oxidization on the electronic, optic, and magnetic properties of InP nanowires have been investigated theoretically [32, 33].

This study has been carried out to determine the effect of H passivation of InP nanowire, which has the zinc-blende structure, and to understand the changes in the electronic structure by substituting Si and Ge atoms separately. The results of the first principles calculations of electronic and structural properties of unpassivated, hydrogen passivated, Si and Ge doped the hydrogen passivated InP nanowires are presented.

2. Modeling and calculation details

The calculations have been done with the Quantum Espresso package simulation code using the density functional theory (DFT) [34-36] within the generalized gradient approximation (GGA) for the exchange-correlation potential, where the electron-ion interactions are defined by Perdew, Burke, and Ernzerhof (PBE) [37]. Convergence with respect to the plane-wave cutoff energy and k-point sampling has been determined carefully. The cutoff energy for the plane wave basis set is taken 40 Ry for all InP NWs. For the Brillouin zone integration, Monkhorst–Pack special k-points, equivalent to the 1 × 1 × 6 mesh, are employed [38]. All the geometries have been optimized until the forces are less than 0.025 eV $A^{\circ -1}$. Firstly, the lattice constant has been determined by geometric optimization of the bulk structure of InP in the zinc blende structure. Then, the zinc blende InP nanowire, with approximately 1.5 nm diameter, is modeled along [111] crystallographic direction using optimized bulk parameters. In order to eliminate the surface effect and neutralize the surface charge, all dangling bonds on the surface of the InP nanowire are passivated by hydrogen atoms. The top and the side views of the original and H-passivated InP nanowire models are shown in Fig. 1. The H-passivated nanowire model contains 37 In atoms, 37 P atoms, and 42 H atoms. Also, the unit cell of the nanowire is shown in the red frame in Fig. 1c. The nanowire is considered to be infinitely long in the z-direction, and a vacuum space (15 Å) is set to avoid the interaction between neighboring nanowires under the periodic boundary conditions.

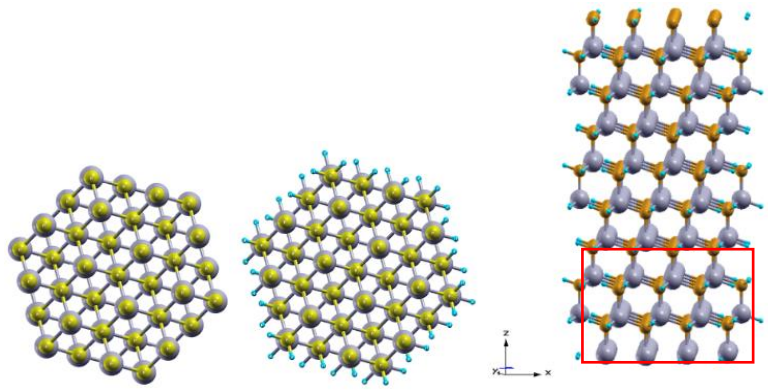

(a) *(b)* *(c)*

Fig. 1. Top views of initial a) unpassivated pure, and b) H-passivated pure, c) side view of H-passivated pure InP NWs (The yellow, grey, and blue balls represent In, P, and H atoms, respectively) (color online)

Fig. 2 shows the hexagonal cross-sectional view of pure H-passivated and non-passivated InP nanowires after geometry optimization.

Si and Ge doped InP nanowires given in Fig. 3 are modeled by replacing an In atom with a Si and a Ge atom from the H-passivated InP NW shown in Fig. 1b and 1c.

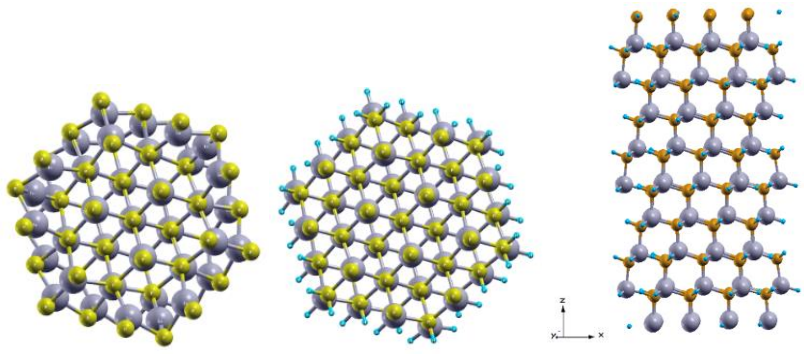

(a) *(b)* *(c)*

Fig. 2. Top views of a) unpassivated pure, and b) H-passivated pure, c) side view of H-passivated pure InP NWs after geometry optimization (color online)

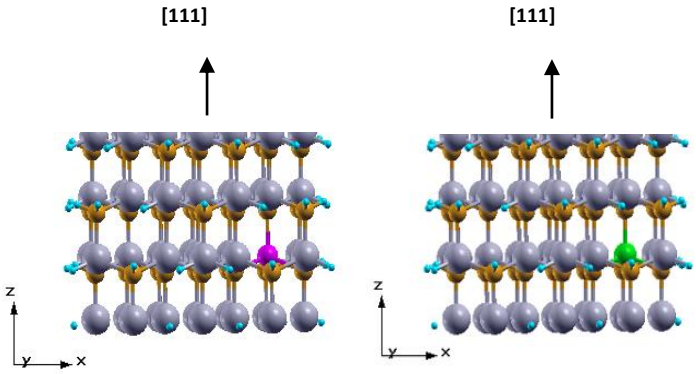

Fig. 3. Side views of H-passivated with a) Si doped b) Ge doped InP NW unit cells (purple and green balls show Si and Ge atoms, respectively) (color online)

3. Results and discussions

Firstly, the accuracy of the calculations has been checked by determining the electronic and structural properties of zinc blende (ZB) bulk InP. After determining the equilibrium state lattice constant of the InP bulk structure, the electronic band structure and density of states (DOS) seen in Fig. 4 have been calculated. The calculated lattice constant and energy band gap are given in Table 1 in comparison with the literature. The bond length between the In and P atoms has been calculated as 2.582 Å. The angle between In-P-In atoms has been determined as 109.471°.

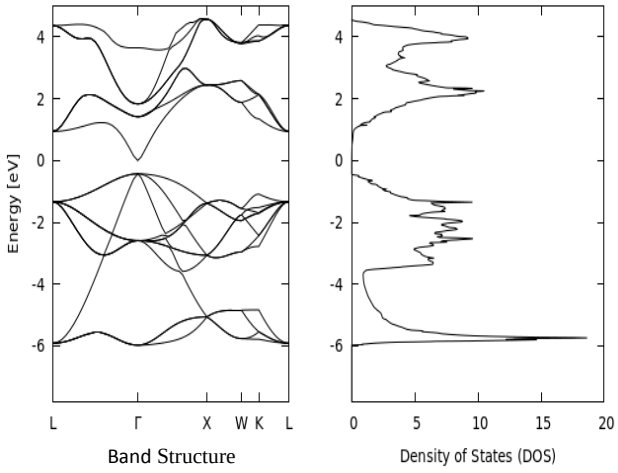

Fig. 4. Band structure and density of states for ZB InP

Table 1. Lattice constants and energy band gaps of ZB InP bulk structure

Parameters	This study	Experimental studies	Other theoretical studies
Lattice constant (Å)	6.01	5.86 [39, 40] 5.85 [41]	6.01 [42] 5.99 [43] 5.97 [44] 5.85 [42] 5.84 [45] 5.65 [43]
Energy gap (eV)	0.43	1.46 [46] 1.42 [47]	0.84 [43] 0.56 [42] 0.52 [45] 0.45 [44] 0.26 [42]

The present lattice constant of ZB bulk InP is found as 6.01Å, which agrees with both previous theoretical and experimental studies [39-43]. Also, the energy band gap is calculated as 0.43 eV, which is consistent with the theoretical studies [42-45]; however, it is seen that a smaller value is obtained when compared with the experimental values [46, 47]. This is caused that DFT calculations usually underestimate the band gap of materials [48]. It can be seen from Fig. 4 that InP has a direct band gap. The conduction band minimum (CBM) and the valence band maximum (VBM) appear in the symmetry point Γ of the Brillouin zone, and the Fermi level is set as zero energy.

First of all, using these parameters obtained for the InP bulk structure, the pure InP nanowire (unpassived and undoped) shown in Fig. 1a has been modeled. Then, after geometrical optimization, the positions of In and P atoms in the nanowire have been determined. It is seen from Fig. 2a that while the In atoms on the surface have moved inward, the P atoms have moved out due to electronegativity after geometry optimization. The movement of atoms depends on their electronegativity, and In atoms are less electronegative than P atoms. So, the radial compression from In atoms is smaller than the radial expansion from P atoms. In and P atoms on the nanowire surface tend to bond and move due to their dangling bonds, but the In and P atoms, far from the surface region and close to the nanowire center, maintain their positions.

On the other hand, when looking at the H-passivated nanowire given in Fig. 2b, it is seen that the shape of the nanowire after optimization is closer to the initial form (Fig. 1.b) compared to the unpassivated nanowire. This is because In and P atoms have behaved in such a way that they do not distort the nanowire shape. The shape of the nanowire has not changed much because the saturation of the surface atoms with hydrogen atoms makes the nanowire surface more stable. In addition, it is observed that after the optimization, the atoms in the inner region of the nanowire have remained motionless, and the hydrogen bonded surface In atoms have moved slightly outwards.

An In atom in the nanowire shown in Figs. 2b and 2c is removed and doped by replacing it with a Si atom. The same process has been carried out for the Ge atom doping. The optimized forms of doped nanowires are shown in Fig 3.

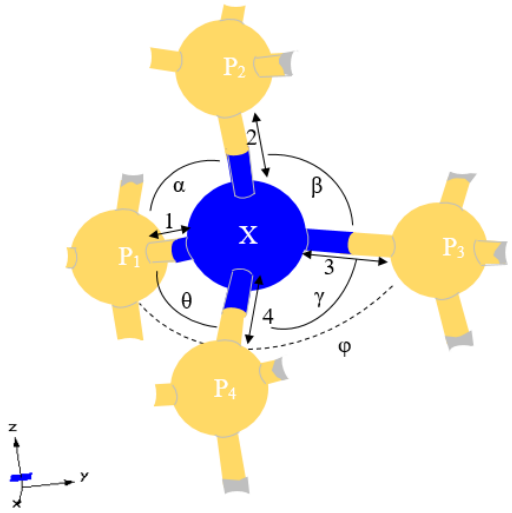

Fig. 5. The bond lengths of X doped atom and bond angles in the nanowires (X= In, Si, and Ge atoms) (color online)

Fig. 5 shows the bond lengths and bond angles (P-X-P) of the X atom with neighboring P atoms in the nanowire. The X atom represents the In atom for the undoped nanowire and the Si or Ge atom for the doped nanowire. The bond lengths and bond angles obtained after optimization for all nanowire structures are listed in Table 2 and Table 3.

Table 2. The bond lengths of X doped atom with P atom (X denotes In, Si, and Ge atoms)

InP NW	X-P Bond Length (Å)			
	1	2	3	4
Unpassivated (X=In)	2.581	2.580	2.647	2.565
H-passivated (X=In)	2.574	2.563	2.570	2.602
H-passivated (X=Si)	2.288	2.303	2.300	2.301
H-passivated (X=Ge)	2.458	2.462	2.488	2.510

As shown in Table 2, the bond length between Si and P_1 atoms given with the number 1 in the Si doped H-passivated nanowire has the shortest bond length value. The longest bond length value is between the In and P_3 atoms in the undoped and unpassivated nanowire, given by the number 3. In addition, the bond angles are given in Table 3.

Table 3. The bond angles of X doped atom with P atoms (X denotes In, Si, and Ge atoms)

InP NW	Bond Angles (°)				
	α (P_1-X-P_2)	β (P_2-X-P_3)	γ (P_3-X-P_4)	θ (P_1-X-P_4)	φ (P_1-X-P_3)
Unpassivated (X=In)	106.890	109.051	110.589	120.699	101.046
H-passivated (X=In)	109.605	108.192	110.946	105.845	112.878
H-passivated (X=Si)	111.683	109.775	107.215	106.155	113.413
H-passivated (X=Ge)	108.838	108.012	113.072	104.125	112.477

The largest angle is the θ (P_1-X-P_4) angle in the undoped and unpassivated nanowire and has been determined as 120.699°. The angle φ (P_1-X-P_3) in the same nanowire has also been determined as 101.046° and has the smallest angle value.

The electronic band structures of the pure and doped InP nanowires are shown in Fig 6. The Fermi level is fitted at zero energy and denoted by the horizontal red line.

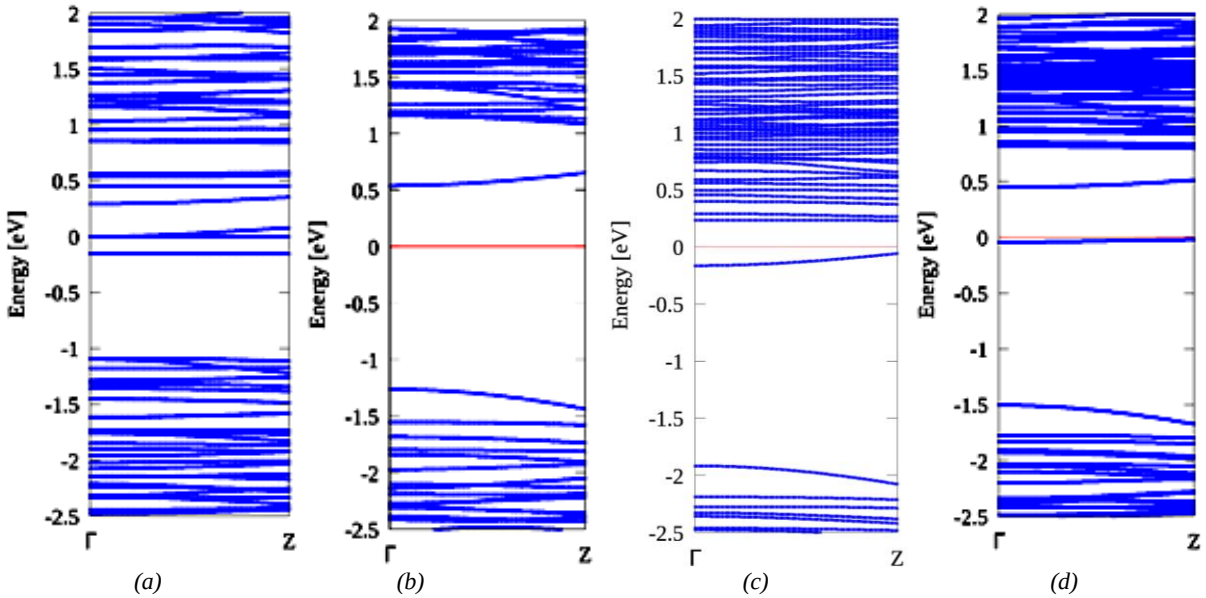

Fig. 6. Band structures for a) pure and unpassivated, b) pure and H-passivated, c) Si doped and H-passivated, d) Ge doped and H-passivated InP nanowires (color online)

We firstly present the electronic band structure for pure and unpassivated InP nanowire oriented [111] direction in Fig. 6a. The presence of the electronic states produced by dangling bonds in the Fermi level region where at below the CBM and also above the VBM is remarkable. When the H passivated undoped nanowire given in Fig. 6b is examined, it is seen that H passivation removes the bands caused by dangling bonds, and the band gap is measured as 1.80 eV. It is clearly seen that the energy band gap opens up because the surface states remain in the conduction and valence bands. The electronic energy bands of the Si doped InP nanowire are given in Fig. 6c. The band gap, which is found as 1.79 eV, was slightly narrowed compared to the undoped InP nanowire, and it is observed that the VBM and CBM shifted to lower energy. The Fermi level enters the conduction band, induces a donor level, and indicates the n-type characteristic. The energy band diagram of the Ge doped InP nanowire given in Fig. 6d shows that the Ge doping generates a donor level at the bottom of the conduction band and creates an n-type semiconductor, in which the electronic conductivity is stronger. The band gap is determined as 1.49 eV is narrower than that of the Si doped InP nanowire band gap. Similar to the Si doped nanowire, VBM, and CBM energy values shift to lower energy levels in Ge doped nanowire. This energy shifting is less in the Ge doped nanowire.

The density of states (DOS) and the partial density of states (PDOS) of pure and doped InP nanowires are shown in Fig. 7, Fig. 8, and Fig. 9. The zero energy levels represent the Fermi level. The valence electrons of the elements have been considered in order to plot the DOS and PDOS. The valence electrons configurations in the pseudopotentials are $4d^{10}5s^25p^1$, $3s^23p^3$, $3s^23p^{2,}$ and $3d^{10}4s^24p^2$ for In, P, Si, and Ge elements, respectively.

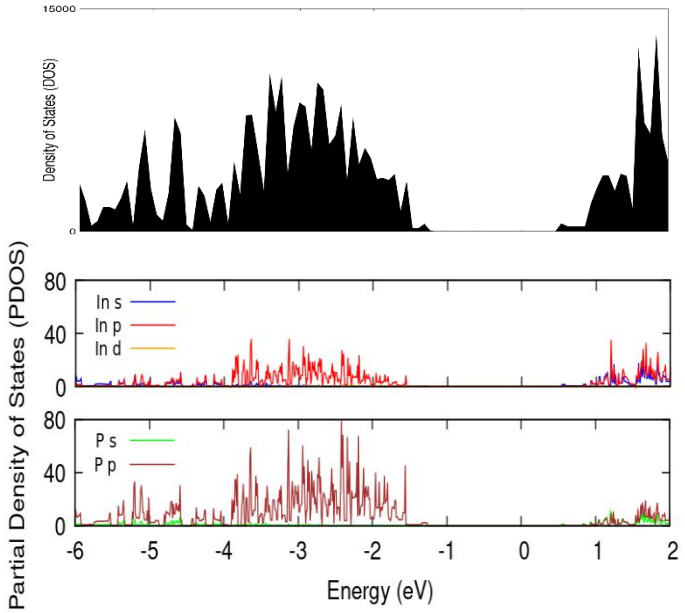

Fig. 7. The density of states (DOS) and the partial density of states (PDOS) for pure InP nanowire (color online)

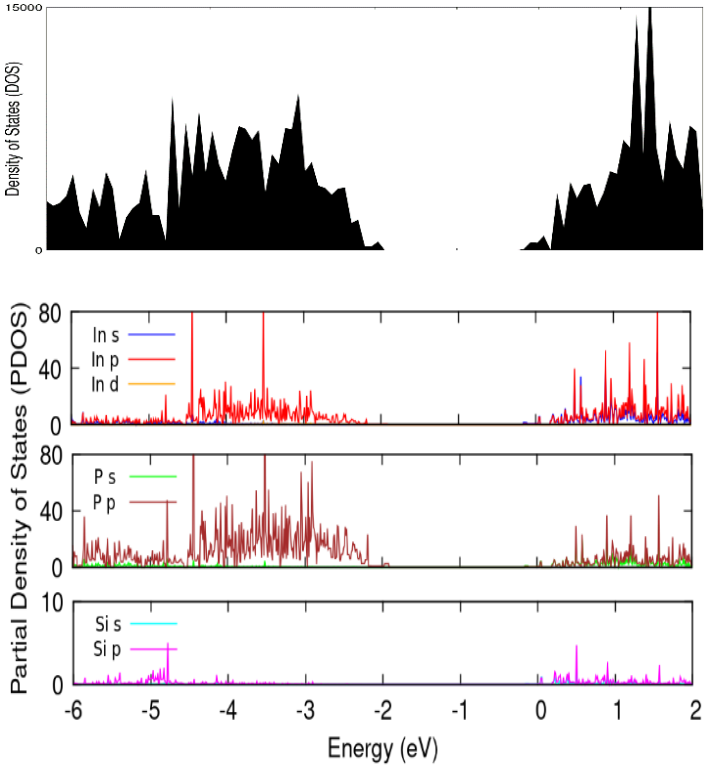

Fig. 8. The density of states (DOS) and the partial density of states (PDOS) for Si doped InP nanowire (color online)

The density of states and the partial density of states for pure H-passivated InP nanowire is given in Fig. 7. For this nanowire, the conduction band is composed of In-s, p and P-s, p electronic states, and the top of the valence band comes from In-p and mainly P-p electronic states. After the Si doping, the VBM and CBM values in the DOS and PDOS graphs in Fig. 8 shift towards lower energy levels as in the energy band graph. The electronic states on the valence bands are mainly formed by In-p and P-p states, and the p orbitals of the In, P, and Si atoms contribute to the conduction bands. Besides, the band localization originating from In-s, p, P-s, p, and Si-s, p orbitals is observed around the Fermi level. When the DOS and PDOS graphs of the Ge-doped nanowire given in Fig. 9 are examined, it is seen that the upper part of the valence bands consists of In-p and P-p electronic states. It is observed that the conduction band is formed mainly by the p orbitals of the In and P atoms, but a small contribution also comes from the In-s, P-s, and Ge-p states. A sharp peak appears composed of mainly Ge-s electronic state, also P-p and slightly In-p electronic states near the Fermi level.

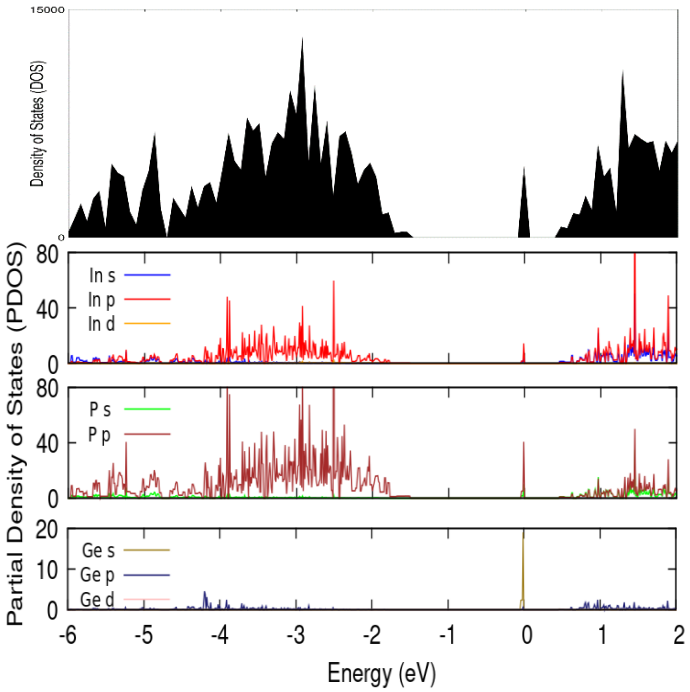

Fig. 9. The density of states (DOS) and the partial density of states (PDOS) for Ge doped InP nanowire

4. Conclusion

A first principles study on the effect of Si and Ge substitutional doping on the electronic and structural properties of hydrogen passivated InP nanowire along the [111] direction with a diameter of 1.5 nm is reported. Bond lengths and bond angles have been determined for all nanowires. The energy band structures, DOS and PDOS have been presented, and the results show that the InP nanowire exhibits a semiconductor characteristic. The H passivation removes dangling bonds, and the band gap opens up because the surface states remain in the conduction and valence bands. The doping with Si and Ge atoms narrows the band gap, and this narrowing is more noticeable in Ge-doped InP nanowires. It is seen that the Si doping shifts the VBM and CBM to the lower energy levels, and this energy decrease is less in the Ge doped nanowire. It is observed that the Si and Ge doping induce donor levels. DOS and PDOS are calculated for pure and doped nanowires, and it is seen to be compatible with the band structures. PDOS analyses show that VBM and CBM occur mainly from the p orbitals of the In and P atoms. The presence of electronic states at the Fermi level for doped nanowires contributes to the n-type semiconductor. The results of these calculations can provide a reference for n-type doping used in electronic applications.

Acknowledgments

The numerical calculations reported in this paper were partially performed at TUBITAK ULAKBIM, High Performance and Grid Computing Center (TRUBA resources).

References

[1] Z. L. Wang, J. Song, Science **312**, 242 (2006).
[2] A. I. Persson, M. T. Bjork, S. Jeppeesen, J. B. Wagner, L. R. Wallenberg, L. Samuelson, Nano Lett. **6**, 403 (2006).
[3] L. N. Quan, J. Kang, C. Z. Ning, and P. Yang, Chem. Rev. **119**, 9153 (2019).
[4] D. J. Carter, J. D. Gale, B. Delley, C. Stampfl, Physical Review B **77**, 115349 (2008).
[5] S. G. Ozkapi, B. Ozkapi, H. Ozkisi, S. Dalgic, Materials Today: Proceedings **4**, 11644 (2017).
[6] C. L. dos Santos, P. Piguini, Physical Review B **81**, 075408 (2010).
[7] K. Nakamura, Jpn. J. Appl. Phys. **54**, 06FJ11 (2015).
[8] S. G. Ozkapi, B. Ozkapi, S. Dalgic, Materials Sciences Forum **916**, 69 (2018).
[9] H. Ozkisi, B. Ozkapi, S. G. Ozkapi, S. Dalgic, Materials Today: Proceedings **4**, 11640 (2017).
[10] P. Srivastava, A. Kumar, N. K. Jaiswal, Superlattices and Microstructures **92** 134 (2016).
[11] Y. Diao, L. Liu, S. Xia, Physics Letters A **383**, 202 (2019).
[12] S. Shen, W. Shen, S. Liu, H. Li, Y. Chen, H. Qi, Materials Today Communications **23**, 100847 (2020).
[13] N. Bouarissa, Phys. B **406**, 2583 (2011).
[14] P. L. Souza, P. R. Ribas, J. V. Bellini, W. M. Mendes, J. Appl. Phys. **79**, 3482 (1996).
[15] M. S. Gydiksen, L. J. Lauhon, J. F. Wang, D. C. Smith, C. M. Lieber, Nature **415**, 617 (2002)
[16] S. Hirano, N. Takeuchi, S. Shu, K. Masuya, J. Appl. Phys. **98**, 1897 (2005).
[17] J. Wallentin, M. Ek, L. R. Wallenberg, L. Samuelson, M. T. Borgstrom, Nano Lett. **12**, 151 (2012).
[18] J. Sun, Y. Yin, M. Han, Z. X. Yang, C. Lan, L. Liu,

Y. Wang, N. Han, L. Shen, X. Wu, J. C. Ho, ACS Nano **12**, 10410 (2018).
[19] H. Yu, J. Li, R. A. Loomis, L. W. Wang, W. E. Buhro, Nat. Mater. **2**, 517 (2003).
[20] R. S. Wagner, W. C. Ellis, Appl. Phys. Lett. **4**, 89 (1964).
[21] Q. Gao, V. G. Dubrovskii, P. Caroff, J. Wong–Leung, L. Li, Y. N. Guo, L. Fu, H. H. Tan, C. Jagadish, Nano Lett. **16**, 4361 (2016).
[22] J. M. Bao, D. C. Bell, F. Capasso, J. B. Wagner, T. Mårtensson, J. Tragårdh, L. Samuelson, Nano Lett. **8**, 836 (2008).
[23] K. Pemasiri, M. Montazeri, R. Gass, L. M. Smith, H. E. Jackson, J. Yarrison-Rice, S. Paiman, Q. Gao, H. H. Tan, C. Jagadish, X. Zhang, J. Zou, Nano Lett. **9**, 648 (2009).
[24] R. E. Algra, M. A. Verheijen, M. T. Borgstroem, L. F. Feiner, G. Immink, W. J. P. van Enckevort, E. Vlieg, E. P. A. M. Bakkers, Nature **456**, 369 (2008).
[25] Q. H. Xiong, J. Wang, P. C. Eklund, Nano Lett. **6**, 2736 (2006).
[26] M. Dunaevskiy, P. Geydt, E. Lahderanta, P. Alekseev, T. Haggren, J. P. Kakko, H. Jiang, H. Lipsanen, Nano Lett. **17**, 3441 (2017).
[27] S. Paiman, Q. Gao, H. H. Tan, C. Jagadish, K. Pemasiri, M. Montazeri, H. E. Jackson, L. M. Smith, J. M. Yarrison–Rice, X. Zhang, J. Zou, Nanotechnology **20**, 225606 (2009).
[28] N. Chauvin, A. Mavel, G. Patriarche, B. Masenelli, M. Gendry, D. Machon, Nano Lett. **16,** 2926 (2016).
[29] D. Li, Z. Wang, F. Gao, Nanotechnology **21**, 505709 (2010).
[30] T. Akiyama, K. Nakamura, T. Ito, Physical Review B **73**, 235308 (2006).
[31] M. D. Moreira, P. Venezuela, T. M. Schmidt, Nanotechnology **19**, 065203 (2008).
[32] T. M. Schmidt, Phys. Rev. B **77**, 085325 (2008).
[33] Z. Yang, H. Chen, Y. Hou, F. Wu, J. Qiao, F. Pan, Physica B **640**, 41402 (2022).
[34] P. Giannozzi, S. Baroni, N. Bonini, M. Calandra, R. Car, C. Cavazzoni, D. Ceresoli, G. L. Chiarotti, M. Cococcioni, I. Dabo, J. Phys. Cond. Mat. **21**, 39 (2009).
[35] P. Hohenberg, W. Kohn, Phys Rev B **136**, 864 (1964).
[36] W. Kohn, L. J. Sham, J. Phys. Rev. A **140**, 1133 (1965).
[37] J. P. Perdew, K. Burke, M. Ernzerhof, Phys. Rev. Lett. **77**, 3865 (1996).
[38] H. J. Monkhorst, J. D. Pack, Phys. Rev. B **16**, 1748 (1977).
[39] O. Madelung, L. Bornstein, Semiconductors, Physics of Group IV Elements and III-V Compounds **17**, New Series, Group III, Springer Verlag, Berlin, 1982.
[40] S. M. Sze, Physics of Semiconductor Device, Wiley Interscience Publication, New York, 1981.
[41] T. Martensson, M. Borgstrom, W. Seifert, B. Ohlsson, L. Samuelson, Nanotechnology **14**, 1255 (2003).
[42] M. Ameri, A. Bentouaf, M. Doui-Aici, R. Khenata, F. Boufadi, A. Touia, Mater. Sci. Appl. **2**, 729 (2011).
[43] D. Shan, Z. Feng, Chin. Phys. B **21**, 1 (2012).
[44] M. G. Brik, A. Kaminska, A. Suchocki, Journal of Applied Physics **108**, 103520 (2010).
[45] F. Kalarasse, B. Bennecer, A. Mellouki, L. Kalarasse, Comput. Mater. Sci. **43**, 791 (2008).
[46] O. Madelung, Semiconductors: Data Handbook, Springer, Berlin, 2004.
[47] R. W. G. Wyckoff, Crystal Structures, 2nd ed., Krieger, Malabar, 1986.
[48] A. Dittmer, R. Izsak, F. Neese, D. Maganas, Inorg. Chem. **58** 9303 (2019).

*Corresponding author: senaguler@trakya.edu.tr